Mechanical Property Characterization of LPCVD Silicon Nitride Thin Films at Cryogenic Temperatures

Wen-Hsien Chuang, *Student Member, IEEE*, Thomas Luger, Rainer K. Fettig, and Reza Ghodssi, *Member, IEEE*

***Abstract*—T-shape, LPCVD silicon nitride cantilevers are fabricated to determine Young's modulus and fracture strength of silicon nitride thin films at room and cryogenic temperatures. A helium-cooled measurement setup is developed and installed inside a focused-ion-beam (FIB) system. A lead-zirconate-titanate (PZT) translator powered by a function generator and a dc voltage is utilized as an actuator, and a silicon diode is used as a temperature sensor in this setup. Resonant frequencies of identical cantilevers with different "milling masses" are measured to obtain thickness and Young's modulus of the silicon nitride thin films, while a bending test is performed to obtain fracture strength. From the experiment, the average Young's modulus of low-pressure chemical-vapor deposition (LPCVD) silicon nitride thin films varies from 260.5 GPa at room temperature (298 K) to 266.6 GPa at 30 K, and the average fracture strength ranges from 6.9 GPa at room temperature to 7.9 GPa at 30 K. The measurement setup and technique presented here can be used to characterize the mechanical properties of different MEMS materials at cryogenic temperatures. [1142]**

***Index Terms*—Cryogenic temperatures, focused-ion-beam (FIB), fracture strength, Young's modulus.**

I. Introduction

THE advances of MEMS technologies in sensors, actuators, instruments, and propulsion systems have made it possible to develop MEMS devices for space and low-temperature applications such as microspacecrafts [1], [2], miniature communications satellites [3], meteorological instrumentation [4], and high-pressure check valves in cryogenic coolers [5]. The reduction of power and thermal requirements with miniature size and weight has made MEMS technologies attractive for these applications. Recently, two-dimensional microshutter arrays, used as a programmable field selector for a Multi-Object Spectrometer (MOS) on the James Webb Space Telescope (JWST), have been developed at NASA Goddard Space Flight Center [6], [7]. The microshutter arrays, made of silicon nitride thin films, require cryogenic operation at 30 K to reduce thermal emission into the instrument. Since the JWST operates in outer space without the possibility of human intervention or maintenance, a complete understanding of mechanical properties and reliability issues at cryogenic temperatures is necessary to design MEMS devices for this environment.

There has been a long history for scientists to investigate the material properties of macroscale specimen at cryogenic temperatures [8]. Current research in this field includes applications of superconductivity [9], cryosurgery systems [10], low-temperature biotechnology [11], and cryogenic operation of microelectronics [12]. To extend MEMS applications into cryogenic environments, the mechanical properties of thin film materials at cryogenic temperatures must be investigated. There are several techniques that have been used to measure the mechanical properties of thin-film materials at room temperature. Direct tension test [13] is an effective method to measure the mechanical properties and the corresponding measured data can be easily interpreted. Nevertheless, the requirements for sample alignment and deflection measurement are stringent. In addition, the sample preparation and experiment setup are complicated. A test structure actuated by electrostatic voltage such as in the M-test [14] is another widely used method. The disadvantage is that only conductive materials are suitable for this technique. A probe-based nanoindentation system [15] with load and displacement resolution better than 0.01 μN and 0.1 nm, respectively, has also been extensively utilized to characterize the mechanical properties. An indenter tip is brought in contact with the test structure, possibly damaging it. Hardness and Young's modulus are then calculated from the load-displacement curve. However, all these methods are difficult to implement in a cryogenic environment.

This paper presents the detailed design of the measurement setup with a PZT translator (PI Inc., Model: PL 122.251) and a microneedle installed inside a focused-ion-beam (FIB) system. Instead of using conventional cantilevers, beams with T-shape structures are utilized in this study. The Young's modulus of LPCVD silicon nitride thin films at room temperature and 30 K is characterized by measuring the resonant frequencies with different milling masses (milled by the FIB system), and the fracture strength is obtained by a bending test. The present measurement setup and experimental techniques are suitable for measurement in a large range of temperatures (from room to 20 K) and can be easily extended to characterize a series of MEMS materials.

II. Design of Cryogenic Measurement Setup

The measurement setup is designed to be installed inside a FEI-620 FIB system as shown in Fig. 1. FIB systems have been widely used in the semiconductor industry to repair masks and interconnection wires, to provide mask-less ion implantation, and to study failure mechanisms [16]. Recently, the fabrication of microstructures of various geometries and prototype nanoscale devices [17] have also been successfully

Manuscript received August 14, 2003; revised January 12, 2004. This work was supported by NASA/Goddard Space Flight Center under Grant NAG512011. Subject Editor G. K. Fedder

W.-H. Chuang, T. Luger, and R. Ghodssi are with the Department of Electrical and Computer Engineering and the Institute for Systems Research, University of Maryland, College Park, MD 20742 USA (e-mail: ghodssi@eng.umd.edu).

R. K. Fettig works as an independent consultant.

Digital Object Identifier 10.1109/JMEMS.2004.836815

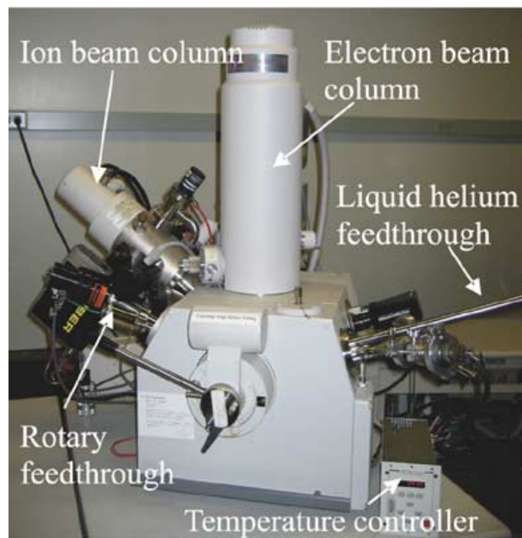

Fig. 1. FIB system with a measurement setup installed inside.

demonstrated using FIB systems. The FEI 620 used in our experiment is a dual beam system, with ion and electron columns, permitting ion milling and *in situ* scanning electron microscopy (SEM). This system also has the ability of depositing platinum (Pt) by ion-induced metal-organic chemical-vapor deposition (MOCVD). These unique capabilities make FIB an appropriate tool for characterizing the mechanical properties of MEMS materials at cryogenic temperatures.

Fig. 2 shows the configuration of the measurement setup inside the FIB system. Liquid helium (LHe) in combination with a resistive thermal source is used to control the temperature from 30 K to room temperature by adjusting the flow rate of LHe and the electrical current flowing through the resistor. Since the measurement setup operates at temperature levels much below ambient temperature, heat transfer is the main concern when designing such a setup [18]. To obtain a cryogenic environment, a thermally isolated device stage with cooling power is required. In our design, the cooling power is provided by a helium diffuser that is connected to a thermally isolated x-y-z stage (rotate-able and tilt-able) with a flexible wire providing a thermal path. Since copper has high thermal conductivity and can be machined easily, the device stage, helium diffuser and thermal path are made from copper. Three G-10 (a continuous filament glass cloth material with an epoxy resin binder) standoffs are used as thermal insulators (thermal conductivity of 0.04 W/m · K at 30 K) to minimize conduction heat transfer between the device stage and the FIB chamber. Due to a high vacuum ($<10^{-5}$ mbar) inside the FIB system, convection heat transfer can be neglected. However, in most cryogenic setups, the primary mode of heat transfer is generally radiant heat transfer. In our design of the radiant shield, an aluminized Mylar layer [19] enclosing the device stage is utilized to reduce radiant heat transfer (see Fig. 3) since the emissivity of aluminized Mylar is lower than that of stainless steel/aluminum oxide chamber wall. There is no thermal conduction path between the Mylar shield and the device stage.

A diode temperature sensor attached to the device stage with thermal response time of 10 ms at 4.2 K and accuracy of 0.25 K at 30 K [20] is utilized to measure the temperature of the chip. The temperature reading and calibration is obtained from a temperature controller [21]. This cryogenic setup has been successfully tested to achieve temperature as low as 20 K with a required cooling time of 16 min. For actuating test devices, a PZT translator powered by a function generator and a DC voltage is attached to a G-10 plate with a stycast epoxy [19]. The G-10 plate is then fixed on a 3-D stage controlled by rotary

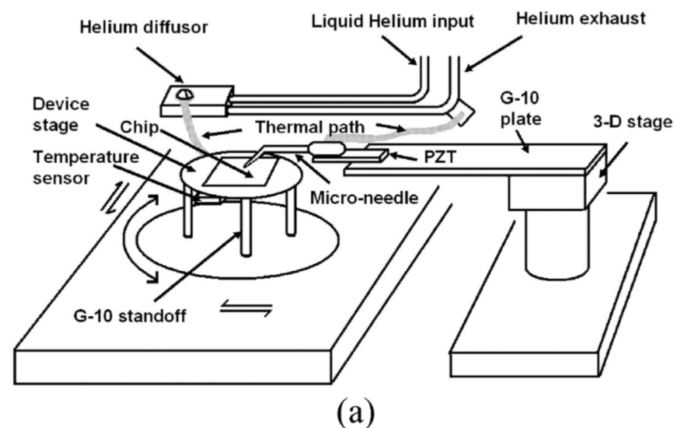

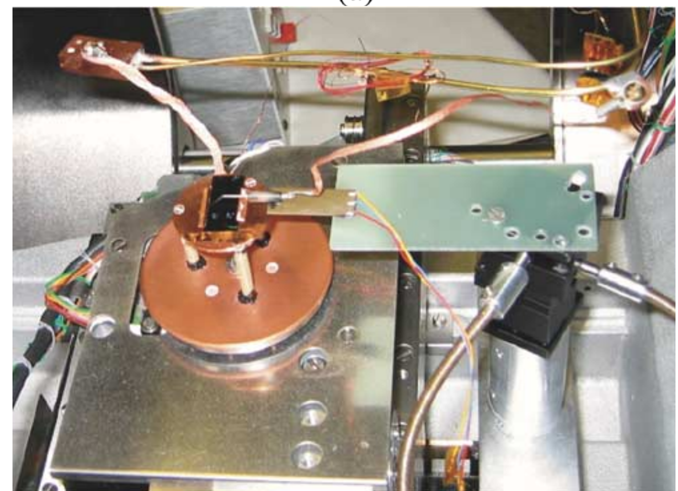

Fig. 2. Configuration of the measurement setup: (a) schematic view and (b) photograph of the system.

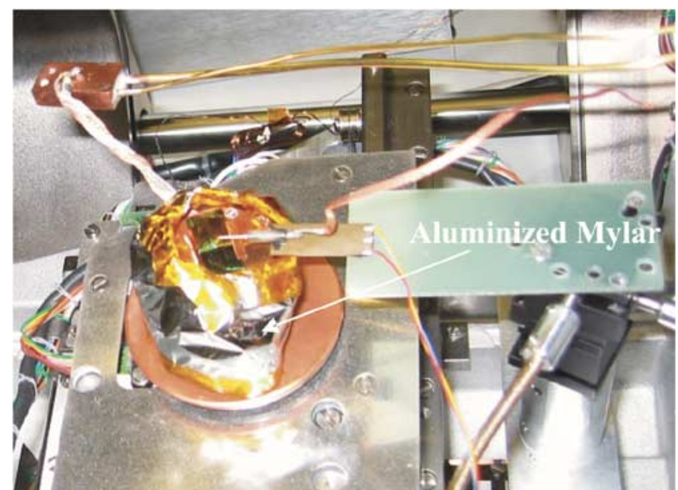

Fig. 3. Measurement setup with three layers of aluminized Mylar shields.

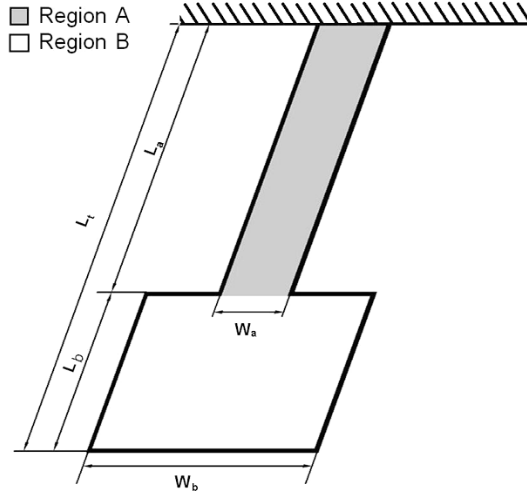

Fig. 4. Schematic diagram of a T-shape cantilever for resonant tests.

feed-throughs. A small G-10 tube (10 mm in length, 3.5 mm in diameter, and 0.6 mm in wall thickness) is attached on the top surface of the PZT translator. A microneedle is mounted to the metal part at the end of this tube. A flexible copper wire (thermal path) cooling the microneedle is soldered to the metal part of the G-10 tube. This configuration prevents malfunction of the PZT translator as it remains warm during cryogenic operation of the microneedle.

III. Device Design and Experimental Technique

A. Young's Modulus of Thin Films

As mentioned earlier, the resonant technique is used to determine the Young's modulus of silicon nitride thin films. Unlike conventional cantilevers, a mass m_b is added to the end of a cantilever as shown in Fig. 4 to form a "spring-mass" system whose first resonant frequency can be measured and computed analytically. The purpose of this design is to reduce the resonant frequency of this T-shape cantilever to a range that can be easily measured. From beam theory, the first resonant frequency of a T-shape cantilever is expressed as [22], [23]

$$f = \frac{1}{2\pi}\sqrt{\frac{3EI}{L^3(m_b + c_1 m_a)}} \tag{1}$$

where $c_1 m_a$(c_1 is a constant and equal to 0.2357) is the effective mass of the cantilever beam in region A, m_b is the added mass of region B, f is the first resonant frequency in Hz, $L = L_a + L_b/2$ is the effective cantilever length, and E is the Young's modulus. The area moment of inertia I is equal to $(w_a t^3)/12$, where w_a is the width of region A, and t is the thickness of the cantilever. Here, T-shape cantilevers are modeled as structures under uniaxial stress. This may violate the condition of biaxial stress at the supporting boundary and lead to error in the expression of the resonant frequency. However, this effect can be neglected due to small introduced error (less than 1.1%) according to finite element analysis simulations.

In our resonant tests, one cantilever is first pushed vertically with the microneedle and then released. The approximate resonant frequency is measured by pointing the electron beam in a fixed position where the vibrating cantilever moves in and out of the electron beam path. This modulates the secondary electron detector signal with the frequency of vibration. This signal is acquired with an oscilloscope and the approximate resonant frequency is determined. Subsequently, the microneedle driven by the PZT translator contacts with the chip and vibrates the cantilever near the frequency determined previously. The frequency is varied over a small range and the response is monitored to determine the exact resonant frequency and the quality factor. Fig. 5. shows the schematic mechanism of the resonant test and Fig. 6. is a SEM picture illustrating that each cantilever vibrates only when the driving frequency of the PZT translator matches with its resonant frequency.

Once the first resonant frequency is determined, the Young's modulus from (1) is given by

$$E = \frac{4\pi^2 f^2 L^3 (m_b + c_1 m_a)}{3I} \tag{2}$$

which is expanded in terms of thickness as follows:

$$E = \frac{16\pi^2 f^2 L^4 \rho}{t^2}\left(\frac{w_b}{w_a}\frac{L_b}{L} + c_1\frac{L_a}{L}\right) \tag{3}$$

where ρ is the mass density. From (3), the dimensions of T-shape cantilevers are critical parameters to calculate Young's modulus. In general, the width and length of a cantilever are determined by layout design of the optical mask and can be measured directly inside the FIB system. On the other hand, the uncertainty of the thin film thickness is the primary source of error for the existing method. To solve this problem, the added mass method has been used to obtain the thickness of a cantilever [24], [25]. A small mass is added to a cantilever and the change in the resonant frequency due to an added mass is measured to calculate the thickness and Young's modulus. The disadvantage of this method is the difficulty to obtain the accurate mass added to the cantilever. Furthermore, to manipulate a bead (mass) on the microscale or nanoscale cantilever is a challenging task.

In contrast, the milling mass approach is introduced in our experiment. The area of the milling mass is determined precisely from the ion-milling pattern. The approximate thickness is estimated from the milling rate and the milling time, measured by the milling of test samples and End Point Detection (EDP) in the FIB system, respectively. If a mass m_i is milled away from the end of a cantilever, the first resonant frequency can be expressed as

$$(m_i - m_b - c_1 m_a) = -\frac{w_a t^3 E}{16\pi^2 L^3}\frac{1}{f_i^2}. \tag{4}$$

The resonant frequencies f_i with different milling mass m_i are measured and the relation between m_i and $1/L^3 fi^2$ is plotted. Here, the change of the effective cantilever length L is calculated by the shift of the center of the mass in region B due to the milling mass m_i. Consequently, the y-intercept yields the effective mass $(m_b + c_1 m_a)$ and thickness of this T-shape cantilever, and the slope gives the Young's modulus.

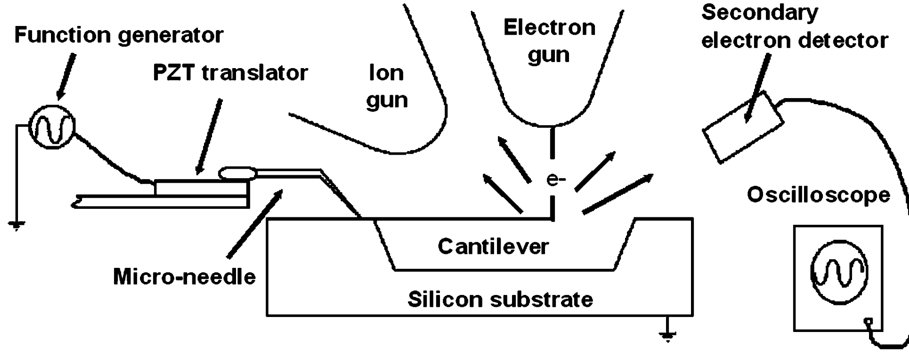

Fig. 5. Schematic diagram of the mechanism for resonant tests.

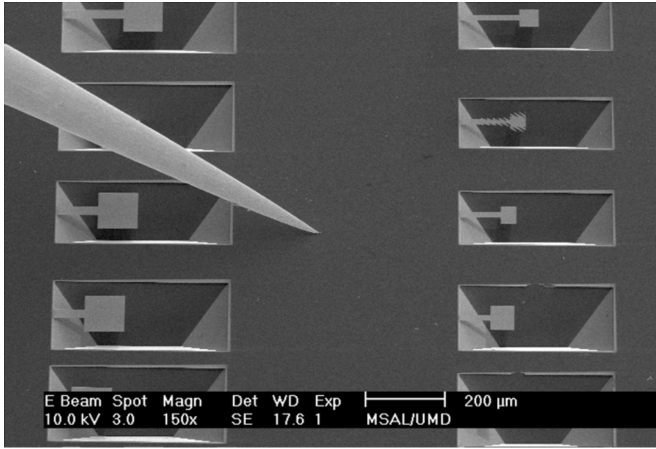

Fig. 6. SEM picture of a vibrating cantilever. Only the second one from top on the right column vibrates because the driving frequency of the PZT translator is near its first resonant mode.

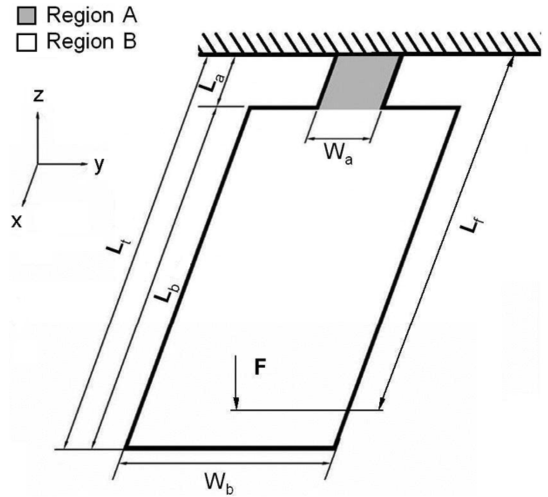

Fig. 7. Schematic diagram of a cantilever for bending tests.

B. Fracture Strengths of Thin Films

For measuring the fracture strength of silicon nitride thin films, bending tests of T-shape cantilevers are performed. The dimensions of the T-shape cantilevers used for bending tests (Fig. 7) are different from those used in the resonant tests. We select the width and length in region B to be larger than those in region A such that region B is rigid relative to region A during the bending test. If a force F is applied to a cantilever at a distance L_f from the fixed end, the inclination θ of the end region A (at $x = L_a$) can be expressed as [22], [23]

$$\theta = \frac{F\left(2L_f L_a - L_a^2\right)}{2EI} \tag{5}$$

where L_a is the length of region A, E is the Young's modulus, and I is the moment of inertial of region A. Equation (5) is valid only when θ is small. If we assume L_f is equal to $nL_a(L_f = nL_a)$, the above equation can be rewritten as

$$\theta = \frac{FL_f L_a}{EI}\left(1 - \frac{1}{2n}\right). \tag{6}$$

Therefore, the maximum moment M about the fixed end of the beam is

$$M = FL_f = \frac{\theta EI}{L_a\left(1 - \frac{1}{2n}\right)}. \tag{7}$$

In our experiment, the large blade of a cantilever (region B) is pushed by the micro-needle through a rotation angle θ. The peak stress occurred at the fixed end and is expressed as

$$\sigma = \frac{Mc}{I} = \frac{\theta Ec}{L_a\left(1 - \frac{1}{2n}\right)} \tag{8}$$

where c is the half thickness of the cantilever. Since the accurate position and force of the micro-needle applied to the cantilever are difficult to measure, the stress determined from (8) has the advantage of being insensitive to the force position if n is large, and the value of the applied force is not needed. The maximum bending angle before failure is measured and the fracture strength of the silicon nitride thin film can be obtained.

IV. Device Preparation

T-shape cantilevers are fabricated using bulk micro-machining techniques. A layer of low-stress LPCVD silicon nitride with an approximate thickness of 0.45 μm and residual stress of 200 MPa is first deposited on a 500-μm-thick silicon substrate. The silicon nitride thin film is then patterned by reactive ion etching (RIE). Finally, the wafer is placed into a 20%, 72 °C potassium hydroxide (KOH) solution [26] for 2.5 hours with uniform agitation to release the T-shape cantilever structures. The etching apparatus sits inside a constant-temperature thermal bath (NESLAB GP-300) with a condenser to keep

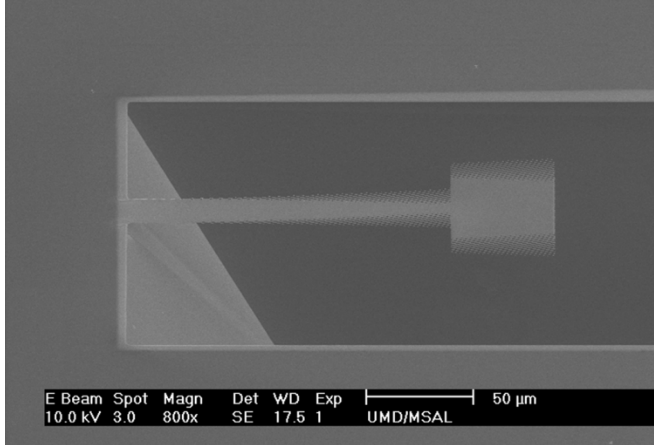

Fig. 8. SEM picture of cantilever 1 at the first resonant mode.

the concentration of KOH steady. A magnet positioned under the solution beaker along with a magnetic stirring bar in the KOH solution is used to produce uniform agitation (1000 rpm). The etch rate from the experiment is 0.79 μm/min. The depth of the etched v-groove is 118.5 μm and the undercut of silicon (lateral etch) is 4 μm.

V. Measurement Results

A. Young's Modulus

Before the resonant test, ion milling is performed to obtain a fixed boundary of the cantilevers, while the dimensions are measured directly inside the FIB system. A T-shape cantilever (cantilever 1) driven to its first resonant mode by the PZT translator is shown in Fig. 8. The vibration amplitude of this cantilever near the resonant frequency is measured and the resulting resonant spectrum is shown in Fig. 9. The quality factor determined from the resonant spectrum is as high as 2050, which is expected due to the high vacuum inside the FIB system. Therefore, the damping effect for Young's modulus extraction can be neglected (the error is less than $3 \times 10^{-6}\%$). Different masses at the end of the cantilever are milled away by the ion-milling function of the FIB system as shown in Fig. 10 and the corresponding resonant frequencies are measured as shown in Table I. Here, a density of $\rho = 3000$ kg/m^3 for LPCVD silicon nitride thin films [27] is used to calculate the milling mass m_i. The relation between m_i and $1/L^3 f_i^2$ is plotted and the equation of a straight line for best fitting is found using Mathematica (version 4.2, software package developed by Wolfram Research Inc.) as shown in Fig. 11. Hence, the extracted thickness and Young's modulus are obtained from the y-intercept and the slope of this straight line, respectively. In our experiments, only one cantilever is milled away several times. For the other cantilevers, a single mass is milled away for the extraction of the thickness and Young's modulus. Table II presents the values of the extracted thickness of the cantilever and the Young's modulus of our LPCVD silicon nitride thin films.

From Table II, the average Young's modulus of low-stress, LPCVD silicon nitride thin films at room temperature is 260.5 GPa with a standard deviation of 5.4 GPa. The Young's modulus of bulk silicon nitride is known to be in the range of 207 to 310 GPa [28]. Schneider and Tucker reported a Young's modulus of 230–265 GPa for 0.2–0.3 μm silicon nitride thin films [29], and Tabata *et al.* obtained 290 GPa for 0.5 μm LPCVD silicon nitride thin films [30]. Therefore, the measured Young's modulus is certainly within the range of the reported values.

After room temperature tests are finished, all cantilevers are cooled down to 30 K in the cryogenic setup and the resonant frequencies of these cantilevers are measured again. The Young's modulus calculated from (4) is shown in Table III and has an average of 266.6 GPa with a standard deviation of 4.1 GPa. Here, the value of 2.3×10^{-6} (K^{-1}) is used as the coefficient of thermal expansion (CTE) of silicon nitride for dimension modification. Although the value of CTE of silicon nitride varies from 1.67×10^{-6} to 2.3×10^{-6} (K^{-1}) [27], [31] and is also a function of temperature, less than 0.1% error is introduced in the calculation of the Young's modulus if only a single value is used. However, the variation of temperature will introduce thermo-mechanical stress and may cause local spring hardening or softening at the supporting boundary. The thermo-mechanical stress can be expressed as [27]

$$\varepsilon_{\mathrm{SiN}} = (\alpha_{T_{\mathrm{SiN}}} - \alpha_{T_{\mathrm{Si}}})\,\Delta T \tag{9}$$

$$\sigma_{\mathrm{SiN}} = \left(\frac{E}{1-\nu}\right)\varepsilon_{\mathrm{SiN}} \tag{10}$$

where $\varepsilon_{\mathrm{SiN}}$ is the thermal strain of silicon nitride, α_T is the CTE, σ_{SiN} is the thermo-mechanical stress of silicon nitride, and ν is Poisson's ratio. If the value of 2.8×10^{-6} (K^{-1}) is used for the CTE of silicon, this thermomechanical stress is found to be -46.4 MPa at 30 K. Since the combination of this thermomechanical stress and the residual stress is still in a range of few hundred MPa, this effect can be ignored with negligible error.

From our measurements, the Young's modulus increases from 260.5 GPa at 298 K to 266.6 GPa at 30 K. The increase of the Young's modulus at low temperature is significant according to the Student T test $(\mathrm{t} = 2.55)$ [32] and can be explained by the fact that the distance of atom or ion separation decreases at low temperature. This distance is determined by the minimum potential energy, i.e., the first derivative of the potential energy is equal to zero. As temperature is decreased, interatomic force (second derivative of the potential energy) tends to increase because of the decrease of atomic distance. Since elastic reaction is due to the action of this force, the Young's modulus increases at lower temperatures.

B. Fracture Strength

A bending T-shape cantilever before and after fracture is shown in Fig. 12. In our experiments, T-shape cantilevers with larger region B are fabricated to make region B relatively rigid to region A and to minimize the measurement error of L_f. Although the deflection at the tip of a cantilever caused by the stress gradient is proportional to the square of the beam length, no obvious bending curvature is found even in our longest cantilever. The dimensions of conventional cantilevers used in bending tests can vary in a large range from mm to nm [33]–[35], mainly determined by the considerations of measurement setups and stress gradients of the beams.

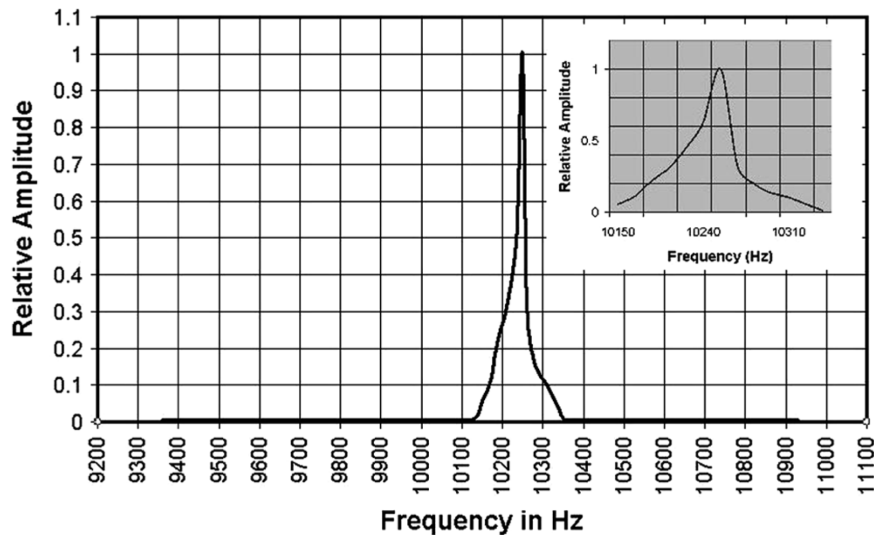

Fig. 9. Resonant spectrum of cantilever 1. The insert is the close-up of the spectrum near the resonant frequency.

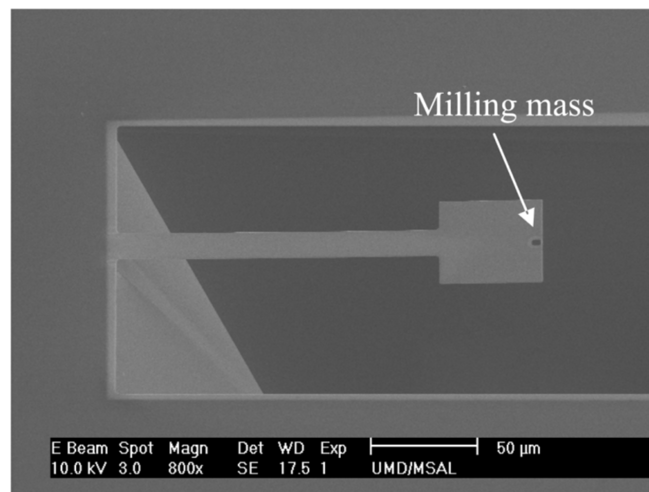

Fig. 10. SEM picture of cantilever 1 with 12.15 pg milling mass.

Several phenomena are observed in our bending tests. First, we find the cantilevers with L_a larger than 3 μm still survive the bending force even when they reach the side walls of the v-grooves as shown in Fig. 13. Second, since the displacement of the cantilever is much larger than its thickness at the fracture point, in-plane stress cannot be neglected. Hence, (8) is not valid in this condition. Third, as mentioned in the section of device preparation, the boundary at the end of the cantilever is floating due to the undercut of silicon in the KOH solution. To accommodate these factors, an ANSYS finite element analysis (FEA) model is developed to obtain accurate fracture strength. Due to the symmetry of a T-shape cantilever, only half of the test specimen is needed in this model. In addition, the curvature of region A caused by the fabrication process is measured and used to simulate the stress concentration of region A.

Instead of measuring fracture angle θ at $x = L_a$, the displacement at $x = L_t$ is determined and used as the input of the FEA model as shown in Fig. 14. From the simulation results, the maximum stress occurs at the edge of region A. Here, the Young's moduli of 260.5 GPa and 266.6 GPa are used for 298 K and 30 K respectively and the Poisson's ratio of 0.23 is used for both temperatures in this model [36]. The fracture strengths of LPCVD silicon nitride at 298 K and 30 K are presented in Table IV. From this table, the average fracture strength at 298 K is 6.9 GPa with a standard deviation of 0.6 GPa. In previous work, Yang *et al.* reported the fracture strength of 12.1 GPa [37] and Coles *et al.* obtained 6.4 GPa [38], both for LPCVD silicon nitride thin films. The difference is mainly caused by different fabrication processes and testing techniques. Hence, the measured fracture strength is still within the range compared with the reported values.

The average fracture strength at 30 K is 7.9 GPa with a standard deviation of 0.7 GPa. The increase of the fracture strength at low temperature can be explained by less thermal agitation. As the temperature is lowered, the atoms in the specimen vibrate less vigorously. A larger applied stress is required to initiate a crack to break the specimen, leading to a higher fracture strength. However, the above explanation is only valid for a defect-free material. For most brittle materials, the fracture strength is determined by stress concentrations from growth

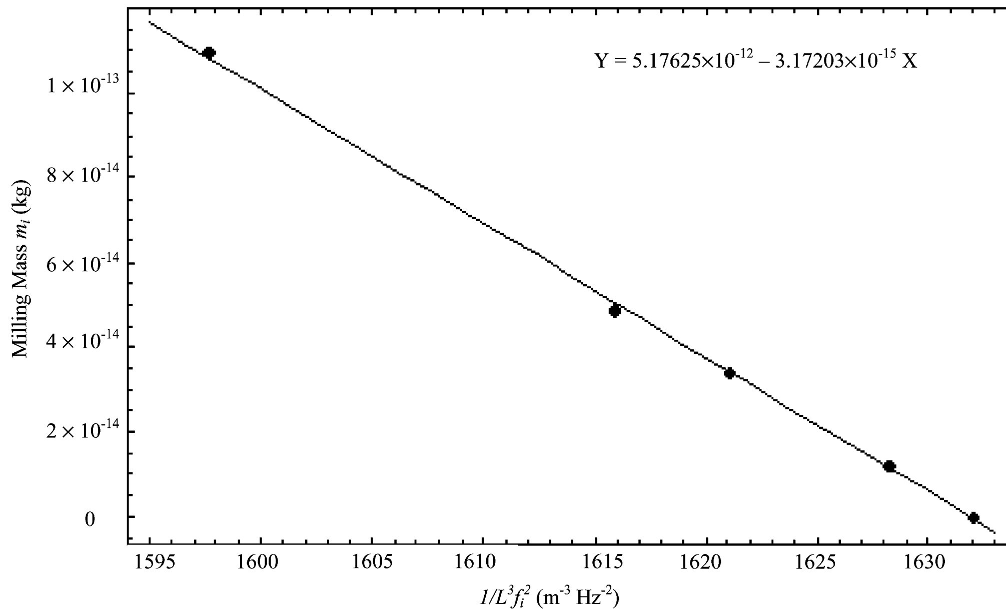

Fig. 11. Linear plot of milling mass m_i versus $(L^3 f_i^2)^{-1}$ for cantilever 1.

TABLE I
DIMENSIONS OF CANTILEVER 1 WITH EFFECTIVE LENGTH AND MEASURED RESONANT FREQUENCY

Cantilever Designation	Dimensions (μm)	Milling Mass m_i (pg)	Effective Length L (μm)	Resonant Frequency f_i (Hz)
1	$L_a = 155$ $W_a = 20$ $L_b = 50$ $W_b = 60$	0	180	10250
		12.15	179.929	10268
		33.75	179.811	10301
		48.6	179.733	10324
		109.35	179.431	10409

TABLE II
DIMENSIONS OF CANTILEVERS WITH EXTRACTED THICKNESS AND YOUNG'S MODULUS

Cantilever Designation	Dimensions (μm)	Extracted Thickness t (μm)	Extracted Young's Modulus E (GPa)
1	$L_a = 155$ $W_a = 20$ $L_b = 50$ $W_b = 60$	0.4625	253.2
2	$L_a = 180$ $W_a = 10$ $L_b = 20$ $W_b = 40$	0.4867	268.8
3	$L_a = 149$ $W_a = 10$ $L_b = 20$ $W_b = 40$	0.4951	262.9
4	$L_a = 229$ $W_a = 20$ $L_b = 50$ $W_b = 100$	0.4800	265.4
5	$L_a = 178$ $W_a = 20$ $L_b = 60$ $W_b = 80$	0.4849	255.7
6	$L_a = 178$ $W_a = 30$ $L_b = 50$ $W_b = 75$	0.4572	258.9
7	$L_a = 129$ $W_a = 20$ $L_b = 40$ $W_b = 50$	0.4508	263.2
8	$L_a = 104$ $W_a = 20$ $L_b = 40$ $W_b = 60$	0.4491	256.2

flaws, yet their variations at cryogenic temperatures are still not clear.

TABLE III
RESONANT FREQUENCY AND EXTRACTED YOUNG'S MODULUS AT 298 K AND 30 K

Cantilever Designation	Resonant Frequency at 298 K (Hz)	Young's Modulus at 298 K (GPa)	Resonant Frequency at 30 K (Hz)	Young's Modulus at 30 K (GPa)
1	10409	253.2	10569	261.6
2	12781	268.8	12845	273.1
3	17222	262.9	17332	268.4
4	5096	265.4	5132	269.8
5	7080	255.7	7168	262.5
6	9006	258.9	9110	266.3
7	16221	263.2	16352	268.6
8	19945	256.2	20158	262.8

C. Discussion

From this study, the Young's modulus of LPCVD silicon nitride thin films increases by 2.3% from 298 K to 30 K, while the fracture strength increases by 14.5%. Several uncertainties may cause errors in the extraction of these properties. First, even though the errors introduced from using a single value of CTE and Poisson's ratio is small, exact values at cryogenic temperatures should be obtained to minimize these errors. Second, the cross sections of the test specimens are not perfectly rectangular due to the fabrication process, especially at the smaller widths. This effect is not considered in the FEA model. Third, the temperature of the test cantilever may be different from the temperature measurement of the diode sensor due to thermal resistance between the device chip and copper (device) stage. Furthermore, radiant heat transfer is not zero since the device stage is not wholly enclosed by aluminized Mylar layers. However, the influence of temperature uncertainty is insignificant because of small temperature dependence of the Young's modulus and fracture strength of LPCVD silicon nitride thin films. An inte-

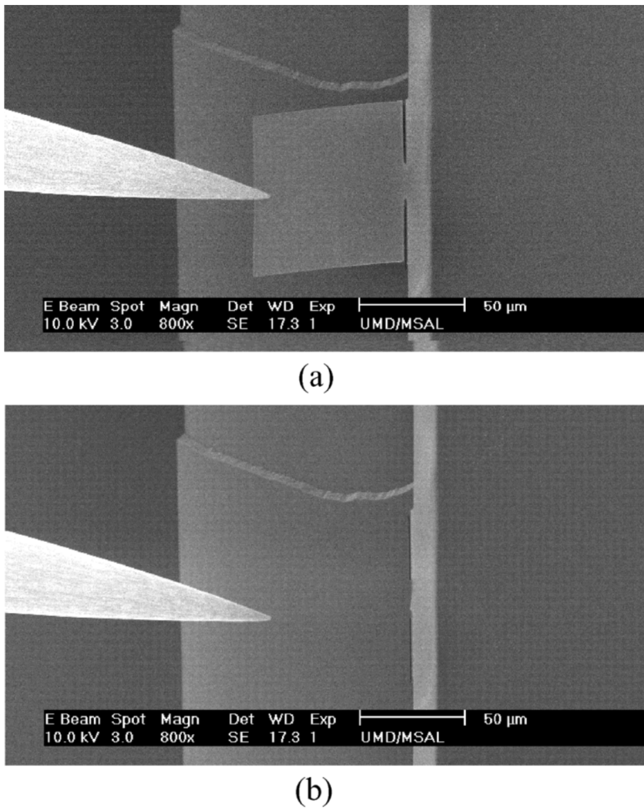

Fig. 12. SEM pictures of a cantilever (a) before and (b) after fracture during the bending test.

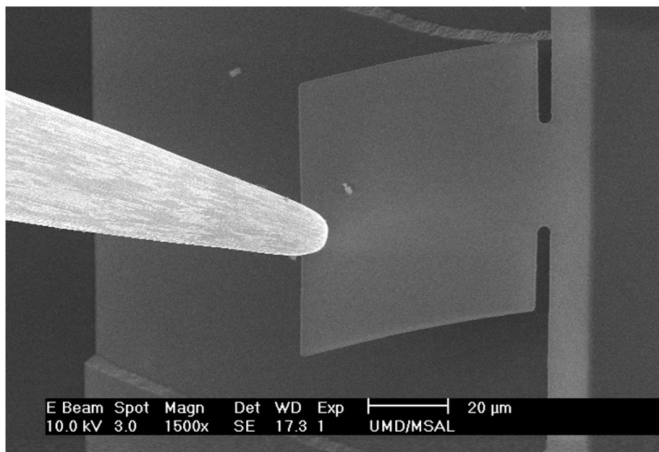

Fig. 13. Bending test of a cantilever with $L_a = 3\ \mu$m.

grated temperature sensor is developed to measure the chip temperature more accurately for further study.

For designing MEMS devices operating at cryogenic temperatures using LPCVD silicon nitride thin films, one can use the values of the Young's modulus and fracture strength at room temperature as the first design parameters. This method is conservative and safe for the first device demonstration. However, for composite structures, the stress caused by the mismatch of CTE at cryogenic temperatures is more pronounced than the change of the Young's modulus and fracture strength, especially for optical MEMS devices requiring flat surfaces. Fig. 15 shows a SEM picture of a microshutter test device at 298 K and 30 K.

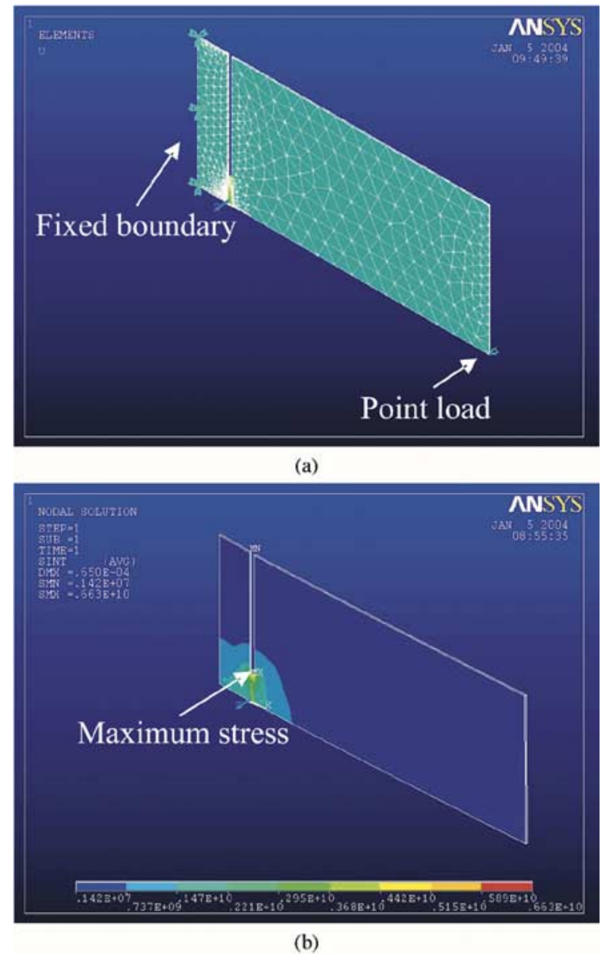

Fig. 14. ANSYS finite element analysis model (a) mesh of the test specimen using "solid 92" element (b) the stress distribution.

The blade of this microshutter is made of silicon nitride, aluminum, and cobalt/iron thin films where it curls up 15 μm at 30 K due to this effect.

VI. Conclusion

This paper presents the design and development of a measurement setup with liquid helium input for mechanical property characterization of thin film materials at cryogenic temperatures. This setup has been successfully tested to achieve temperature down to 20 K. The concept of using T-shape cantilevers instead of conventional ones is discussed and the test specimens are fabricated by bulk micromaching technique, which is a relatively simple process. The resonant test is carried out to obtain the Young's modulus of LPCVD silicon nitride thin films. To determine the thickness of the cantilever, the variation of resonant frequencies with different milling masses is recorded and an analytic model is developed to extract the thickness and Young's modulus simultaneously. The fracture behavior of LPCVD silicon nitride is characterized using the bending test combined with a FEA model.

From the experiment, the Young's modulus of LPCVD silicon nitride thin films varies from 260.5 GPa at 298 K to 266.6 GPa at 30 K, and the fracture strength ranges from 6.9 GPa at 298 K to 7.9 GPa at 30 K. The increase of the

TABLE IV
TEST RESULTS OBTAINED USING ANSYS FEA MODEL WITH BENDING MEASUREMENTS AS INPUTS AT 298 K AND 30 K

Specimen	A	B	C	D	E
Dimensions (μm)	La = 1.0, Wa = 5.0 Lb = 28, Wb = 28 t = 0.45	La = 1.3, Wa = 5.0 Lb = 28, Wb = 28 t = 0.45	La = 1.5, Wa = 15 Lb = 85, Wb = 85 t = 0.45	La = 1.0, Wa = 5.0 Lb = 28, Wb = 28 t = 0.45	La = 1.5, Wa = 15 Lb = 85, Wb = 85 t = 0.45
Test Temperature (K)	298 K	298 K	298 K	30 K	30 K
Average Fracture Strength (GPa)	6.7	7.2	7.1	7.9	8.0
Standard Deviation (GPa)	0.7	0.5	0.6	0.7	0.6
Number of test samples	10	5	10	10	10

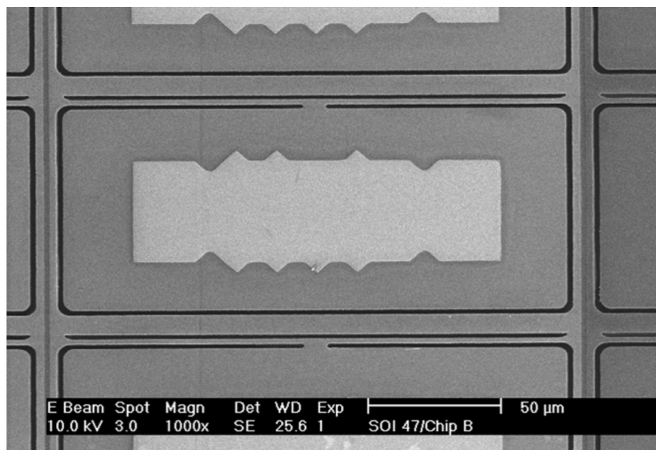

(a)

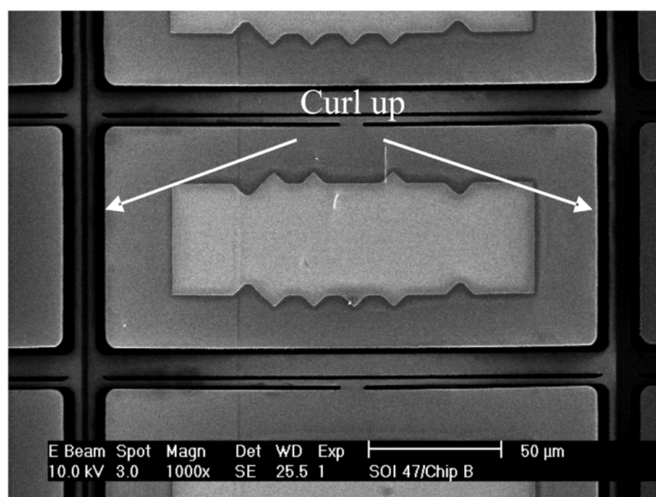

(b)

Fig. 15. SEM pictures of a microshutter device at (a) 298 K and (b) 30 K (The device is fabricated at NASA Goddard Space Flight Center).

Young's modulus and fracture strength is attributed to the decrease in thermal agitation between atoms at cryogenic temperatures. The Poisson's ratio, coefficient of thermal expansion, and fatigue property of LPCVD silicon nitride thin films at cryogenic temperatures are under investigation for further understanding of mechanical property behavior at cryogenic temperatures.

ACKNOWLEDGMENT

The authors would like to thank the microshutter group at NASA Goddard Space Flight Center for their support and help of this project. The staff of the Institute for Research in Electronics and Applied Physics (IREAP) at University of Maryland, especially N. Ballew and J. Barry, are also acknowledged for their help in using the cleanroom facility and the FIB system.

REFERENCES

[1] T. K. Tang, "MEMS for space applications," in *Proc. SOI Conf. 1999*, 1999, p. 67.
[2] Q. A. Shams, M. Moniuszko, and J. C. Ingham, "Applying MEMS technology to field, flight & space deployable systems," in *Proc. Instrumentation in Aerospace Simulation Facilities, 19th International Congress on ICIASF 2001*, Aug. 2001, pp. 246–255.
[3] S. J. Fiedziuszko, "Applications of MEMS in communication satellites," in *Proc. Microwaves, Radar and Wireless Communications. 2000. MIKON-2000. 13th International Conference*, vol. 3, May 2000, pp. 201–211.
[4] D. Farrar, W. Schneider, R. Osiander, J. L. Champion, A. G. Darrin, and D. Douglas, "Controlling variable emittance (MEMS) coatings for space applications," in *Proc. Thermal and Thermomechanical Phenomena in Electronic Systems 2002, the Eighth Intersociety Conference*, May–June 2002, pp. 1020–1024.
[5] J. F. Burger, M. C. van der Wekken, E. Berenschot, H. J. Holland, H. J. M. ter Brake, H. Rogalla, J. G. E. Gardeniers, and M. Elwenspoek, "High pressure check valve for application in a miniature cryogenic sorption cooler," in *Proc. IEEE MEMS 99*, 1999, pp. 183–188.
[6] S. Moseley, R. Fettig, A. Kutyrev, C. Bowers, R. Kimble, J. Orloff, and B. Woodgate, "Programmable 2-dimensional microshutter arrays," in *Proc. SPIE 3878, Micromachining and Microfabrication*, Sept. 1999.
[7] S. Moseley, R. Fettig, A. Kutyrev, M. Li, D. Mott, and B. Woodgate, "Status of the development of a 128 × 128 microshutter array," in *Proc. SPIE 4178, Micromachining and Microfabrication*, Sept. 2000.
[8] R. F. Barron, *Cryogenic Systems*. Cambridge, U.K.: Oxford University Press, 1985.
[9] C. A. Hamilton, D. G. McDonald, J. E. Sauvageau, and S. R. Whitele, "Standards and high-speed instrumentation," *Proc. IEEE*, vol. 77, no. 8, pp. 1224–1232, Aug. 1989.
[10] J. S. Chen, K. Agnissey, T. Shaffer, C. Philips, and M. Wolfson, "Transient heat transfer in human endometrium during cryoablation," in *Proc. IEEE 28th Annual Northeast, Bioengineering Conference 2002*, Apr. 20–21, 2002, pp. 63–64.

[11] A. Devernoe, M. Parizh, G. Rutman, A. Kagan, M. King, G. Ciancetta, R. Wilcox, and B. Winger, "Actively shielded 8 tesla magnet for FT-ICR mass spectrometry," *IEEE Trans. Appl. Superconduct.*, vol. 10, no. 1, pp. 767–770, Mar. 2000.

[12] R. C. Jaeger and F. H. Gaensslen, "Low temperature semiconductor electronics," in *Proc. Thermal Phenomena in the Fabrication and Operation of Electronic Components: I-THERM'88, InterSociety Conference*, May 1988, pp. 106–114.

[13] T. Yi and C. J. Kim, "Measurement of mechanical properties for MEMS materials," *Meas. Sci. Technol.*, vol. 10, pp. 706–716, 1999.

[14] P. M. Osterberg and S. D. Senturia, "M-TEST: A test chip for MEMS material property measurement using electrostatically actuated test structures," *J. Microelectromech. Syst.*, vol. 6, no. 2, pp. 107–118, June 1997.

[15] C. M. Pharr and W. C. Oliver, "Measurement of thin film mechanical properties using nanoindentation," *MRS Bull.*, pp. 28–33, July 1992.

[16] J. Orloff, M. Utlaut, and L. Swanson, *High Resolution Focused Ion Beams: FIB and Its Applications*. New York: Kluwer, 2002.

[17] S. J. Kim, T. Yamashita, K. Y. Lee, M. Nagao, M. Sato, and H. Maeda, "Development of 3-D focused-ion-beam (FIB) etching methods for nano and micro-technology application," in *Proc. Microprocesses and Nano-Technology Conference 2001 International*, Oct.–Nov. 2001, pp. 34–35.

[18] R. F. Barron, *Cryogenic Heat Transfer*. New York: Taylor & Francis, 1999.

[19] G. K. White and P. J. Meeson, *Experimental Techniques in Low-Temperature Physics*, 4th ed: Oxford University press, 2002.

[20] Lake Shore Cryotronics Inc., Model: DT-470-SD-12.

[21] Lake Shore Cryotronics Inc., Model: 321.

[22] W. D. Pilkey, *Formulas for Stress, Strain, and Structural Matrices*. New York: Wiley, 1994.

[23] W. C. Young, *Roark's Formulas for Stress and Strain*. New York: McGraw-Hill, 1989.

[24] J. P. Cleveland, S. Manne, D. Bocek, and P. K. Hansma, "A nondestructive method for determining the spring constant of cantilevers for scanning force microscopy," *Rev. Sci. Instrum.*, vol. 64, pp. 403–405, Feb. 1993.

[25] A. Gupta, J. P. Denton, H. McNally, and R. Bashir, "Novel fabrication method for surface micromachined thin single-crystal silicon cantilever beams," *J. Microelectromech. Syst.*, vol. 12, pp. 185–192, Apr. 2003.

[26] H. Seidel, L. Csepregi, A. Heuberger, and H. Baumgartel, "Anisotropic etching of crystalline silicon in alkaline solution-part II. influence of dopants," *J. Electrochem. Soc.*, vol. 137, pp. 3626–3632, 1990.

[27] S. D. Senturai, *Microsystem Design*. New York: Kluwer, 2001.

[28] D. R. Askeland, *The Science and Engineering of Materials*, 2nd ed. Boston, MA: PWS-KENT, 1989.

[29] D. Schneider and M. D. Tucker, "Non-destructive charaterization and evaluation of thin films by laser induced ultrasonic surface waves," *Thin Solid Films*, vol. 209–291, pp. 305–311, 1996.

[30] O. Tabata, K. Kawahata, S. Sugiyama, and I. Igarashi, "Mechanical property measurements of thin-films using load deflection of composite rectangular membranes," *Sens. Actuators*, vol. 20, pp. 135–141, Nov. 1989.

[31] *Materials Handbook*, 15th ed., 2002. G. S. Brady, H. R. Clauser, and J. A. Vaccari.

[32] F. Mosteller and J. W. Tukey, *Data Analysis and Regression*. Reading, MA: Addison-Wesley, 1977.

[33] P. Hollman, A. Alahelisten, M. Olsson, and S. Hogmark, "Residual stress, Young's modulus and fracture stress of hot flame deposited diamond," *Thin Solid Films*, vol. 270, pp. 137–142, 1995.

[34] T. P. Weihs, S. Hong, J. C. Bravman, and W. D. Nix, "Mechanical deflection of cantilever microbeams: A new technique for testing the mechanical properties of thin films," *J. Mater. Res.*, vol. 3, pp. 931–942, 1988.

[35] T. Namazu, Y. Isono, and T. Tanaka, "Nano-scale bending test of Si beam for MEMS," in *Proc. IEEE Thirteenth Annual Int. Conf. on Micro Electro Mechanical Systems*, 2000, pp. 205–210.

[36] *Handbook of Chemical Vapor Deposition, Principles, Technology, and Applications*, H. D. Pierson, New York, 1999.

[37] J. Yang and O. Paul, "Fracture properties of LPCVD silicon nitride thin films from the load-deflection of long membranes," *Sens. Actuators*, vol. A97–98, pp. 520–526, 2002.

[38] G. Coles, R. L. Edwards, and W. Sharpe, "Mechanical properties of silicon nitride," in *Proc. SEM Annual Conference*, June 2001.

Wen-Hsien Chuang (S'04) received the B.S. and M.S. degrees in electrical engineering from the National Cheng Kung University, Tainan, Taiwan, in 1995 and 1997 respectively.

In August 2001, he joined the MEMS Sensors and Actuators Lab. (MSAL) at University of Maryland and began working toward the Ph.D. degree. His current research, in collaboration with NASA Goddard Space Flight Center (GSFC), focuses on design, fabrication, and cryogenic characterization of MEMS materials and devices for space applications.

Mr. Chuang is a Student Member of the AVS and MRS societies.

Thomas Luger is a graduate student in mechanical engineering at the Technical University Berlin, Germany.

In 2003, he worked as a graduate research assistant in the MEMS Sensors and Actuators Lab. (MSAL) at the University of Maryland at College Park for six months and involved in the project of characterization of mechanical properties of MEMS materials for space applications. Currently, his research focuses on the packaging of microbatteries with parylene.

Rainer K. Fettig received a Diploma in physics and the degree Dr.rer.nat. from the University of Karlsruhe, Germany, in 1986 and 1993, respectively.

Currently, he is an independent scientist working on various aspects of microstructures for space flight applications. Between 1989 and 1996, he headed a team that developed built and delivered thermoelectric infrared detectors for the focal plane 1 of the CIRS instrument on board CASSINI, a NASA mission to Saturn. Between 1996 and 2002, he worked at NASA Goddard Space Flight Center on several projects to develop microstructures for optical applications. He played a major role in the development of microshutters, one of NASA's most visible MEMS projects. In 2002, he returned to Karlsruhe and spent a year at the Research Center Karlsruhe to develop nanohole optical filters produced in a modified LIGA process. He has been freelancing since July 2003.

Reza Ghodssi (S'92–M'97) was born in Tehran, Iran, in 1966. He received the B.S., M.S., and Ph.D. degrees in electrical engineering from the University of Wisconsin at Madison, in 1990, 1992, and 1996, respectively. His Ph.D. dissertation was focused on development of a high aspect ratio microfabrication process for an electrostatic driven MEMS device using X-ray lithography and LIGA technology.

He was a Postdoctoral Associate and a Research Scientist in the Microsystems Technology Laboratories and the Gas Turbine Laboratory at the Massachusetts Institute of Technology (MIT), Cambridge, from 1997 to 1999. During his tenure at MIT, he developed the building block MEMS fabrication technologies for a microturbine generator device and also served as an Assistant Director on that project. In January 2000, he joined the Department of Electrical and Computer Engineering and the Institute for Systems Research at the University of Maryland (UMD) at College Park as an Assistant Professor. His research interests are in design and development of microfabrication technologies and their applications to microsensors, microactuators and integrative microsystems.

Dr. Ghodssi was awarded the 2001 UMD George Corcoran Award, 2002 National Science Foundation CAREER Award and the 2003 UMD Outstanding Systems Engineering Faculty Award. Dr. Ghodssi has served as a program co-chairman for the 2001 International Semiconductor Device Research Symposium (ISDRS) and since 2002 as a chairman of the MEMS and NEMS Technical Group at the American Vacuum Society (AVS). Dr. Ghodssi is a co-founder of the MEMS Alliance Group in the greater Washington area and a Member of the AVS and MRS societies.